Electric double layer capacitance of restricted primitive model for an ionic fluid in slit-like nanopores: A density functional approach

O. Pizio, S. Sokołowski, and Z. Sokołowska

Additional information on J. Chem. Phys.

Electric double layer capacitance of restricted primitive model for an ionic fluid in slit-like nanopores: A density functional approach

O. Pizio,[1,a)] S. Sokołowski,[2] and Z. Sokołowska[3]

[1]*Instituto de Química, Universidad Nacional Autonoma de México, Circuito Exterior, Ciudad Universitaria, México D.F. 04510, México*
[2]*Institute for Multiscale Simulations, Friedrich-Alexander-Universität Erlangen-Nürnberg, D-91052 Erlangen, Germany and Department for the Modeling of Physico-Chemical Processes, Maria Curie-Skłodowska University, 20-031 Lublin, Poland*
[3]*Institute of Agrophysics, Polish Academy of Sciences, Doświadczalna 4, 20290 Lublin, Poland*

We apply recently developed version of a density functional theory [Z. Wang, L. Liu, and I. Neretnieks, J. Phys.: Condens. Matter **23**, 175002 (2011)] to study adsorption of a restricted primitive model for an ionic fluid in slit-like pores in the absence of interactions induced by electrostatic images. At present this approach is one of the most accurate theories for such model electric double layers. The dependencies of the differential double layer capacitance on the pore width, on the electrostatic potential at the wall, bulk fluid density, and temperature are obtained. We show that the differential capacitance can oscillate as a function of the pore width dependent on the values of the above parameters. The number of oscillations and their magnitude decrease for high values of the electrostatic potential. For very narrow pores, close to the ion diameter, the differential capacitance tends to a minimum. The dependence of differential capacitance on temperature exhibits maximum at different values of bulk fluid density and applied electrostatic potential. © *2012 American Institute of Physics*. [http://dx.doi.org/10.1063/1.4771919]

I. INTRODUCTION

The problem of description of ionic fluids in contact with single charged surface, or confined to pores of nanoscopic dimensions with charged walls, is of much importance for basic research, as well as for various applications. In spite of reached progress in understanding of basic features of microscopic structure, thermodynamic and electric properties of these systems in equilibrium, the problem still represents challenge for statistical mechanical theory and computer simulations.

Theoretical modelling of the microscopic structure and thermodynamic properties of homogeneous and inhomogeneous electrolytes is most commonly performed in the framework of the primitive models (PM), in which ions are considered as charged hard spheres with arbitrary diameters and charges. Moreover, in several approaches the simplifying assumption of equality of diameters of ionic species is applied, yielding the restricted primitive model (RPM). In both, the PM and RPM, the solvent subsystem is mimicked by a uniform dielectric continuum characterized by a certain constant value of dielectric susceptibility.

In temporal retrospective, initial theoretical approaches for the description of inhomogeneous (i.e., in an external field or with intrinsically broken symmetry, e.g., in the case of ionic vapor–ionic liquid separation) RPM fluids were based on singlet,[1,2] as well as on second-order[3] integral equations. However, later studies have shown that for confined uncharged,[4] as well as for charged fluids, the density

functional (DF) methods provide an attractive alternative.[5] These theories yield more accurate results comparing to the predictions of the singlet theory. Moreover, they are comparable to the accuracy of second-order integral equations, but are considerably easier to implement. In addition, the density functional approaches permit to study an ample set of thermodynamic properties involving phase equilibria in nonuniform fluid systems with different geometry of confinement, see, e.g., Refs. 6–9.

Usually, in DF theories of nonuniform electrolytes, the ion–ion correlations are divided into the direct Coulomb contribution, the hard-sphere contribution and the electric residual contribution that results from coupling between Coulomb and hard-sphere interactions.[10–16] The difference between various DF approaches is due to different ways of evaluation of the residual contributions. According to the compressibility route approaches,[10–14] the residual contribution is evaluated using a perturbation of the intrinsic Helmholtz free energy around a bulk reference state. The residual free energy functional is calculated then as an integral involving the residual term of the direct pair correlation function. A more sophisticated approach, called "the reference fluid DF theory"[15] introduces a method for defining a "smoothed," nonuniform fluid as the reference state instead of the bulk fluid. However, it also belongs to the compressibility route developments.

In our previous works[16–20] we have proposed and applied the approach that uses nonuniform fluid weighted densities as the reference state and the free energy functional for the residual contribution from the MSA energy route for the bulk equation of state.[21,22] This development can be called "an energy route MSA-based solution." In contrast to the

a)Electronic mail: pizio@unam.mx.

137, 234705-1

compressibility route approaches, the energy route theory is the only method capable to predict ionic gas–ionic liquid transition for confined RPM,[16,17] as well as the existence of a maximum of the double layer capacitance on temperature dependence.[18,19] However, at high temperatures comparing to the critical temperature of the RPM, for quite high bulk electrolyte densities as well as for high wall charges, the microscopic structure of electric double layer predicted by the energy route approach is less accurate than that emerging from some compressibility route theories.[12,23,24]

Our principal focus in the deliberation above was concentrated on the ionic fluid side of the problem that actually involves solid phase as well. Description of the latter solely as a source of an external field is not sufficient in dealing with several important important issues, however.

Recently, the so-called electric double layer capacitors (DLCs) have received much attention[25–30] because of their power delivery performance that fills the gap between dielectric capacitors and traditional batteries. With the growing development of renewable energy sources, these systems are thought to play an important role complementing or even replacing batteries in the energy storage field. The DLCs are microporous solids and their excellent electrochemical performance is mainly due to reversible ion adsorption in porous electrodes.[31–33] It was found that in some cases an anomalous behavior manifested as an increase of the capacitance of DLCs can occur as the pore size decreases and approaches the dimension of ions.[31,32] Moreover, it was observed that dependent on the size of the pores, substantial separation of the positive and negative ions can take place inside the pores.[33,34]

The problem of description of DLCs has been tackled using computer simulations,[33,35–42] as well as theoretical methods.[34,41,43–45] These works made clear an important problem relevant for the description of electrostatic forces in model systems involving different phases. If the solid walls are considered as a dielectric continuum, then the difference of the dielectric constant of the confined fluid (even under simplifying assumption that it is the same as for the fluid in the bulk reservoir) and of solid walls must be taken into account in order to properly work out the ion–ion and ion–charged wall interactions. In other words one has to consider not only the presence of "real" ions but also of their electrostatic images, resulting from the difference in dielectric constants.[35–37,41] The appropriate expressions for the interaction potentials can be derived from classical electrostatics.[46] Of, course, this is not necessary in the framework of an alternative approach, which relies on modelling of a system at entirely molecular level. In other words one should take into account molecular (or atomistic) model for solid walls[42] and the presence of a molecular solvent (e.g., water), if necessary. Unfortunately, while such a method of modelling can be implemented in computer simulations, its application in theoretical approaches would be difficult.

Implementation of the expressions for ionic interactions resulting from continuous electrostatics (involving external field and pair interaction due to images) in the integral equation approaches would require the second-order level of the theory. It is feasible, but prohibitively difficult numerically,

and does not guarantee of accuracy of the results because of approximations involved, see, e.g., Ref. 47 for the statement of the problem. In the case of DF approaches, account of electrostatic images has not been attempted so far, because of methodological problems in constructing the electrostatic free energy functional.

Validity and accuracy of theoretical approaches can be evaluated confronting their results with computer simulations data for a solid wall–RPM fluid interface that have been carried out assuming constancy of the dielectric constant throughout the entire system.[48–50] The aim of computer simulations, as well as of theoretical calculations is twofold. On one hand, theoretical results can be used to get an insight into molecular mechanism of a given phenomenon and to attempt interpretation of the experimental data. Instantaneously, such a comparison permits to evaluate validity of the employed modelling. On the other hand, the calculations performed for well established models can predict new phenomena or relationships between measurable quantities. Validation of a given model is not a simple task. Usually, performing theoretical calculations one applies the simplest model, possible or a minimal model. Even the model that neglects some seemingly essential ingredients of a real system can be useful in interpreting the existing data from other sources and can possess predictive power, like it happens with the RPM in the theory of electrolyte solutions.

The interpretation of the experimental data for DLCs suggested on the basis of computer simulations performed in Refs. 37 and 41 is that the difference in the dielectric constants of the nanopore interior and exterior is the cause of the experimentally observed anomalous behavior of the capacitance.[31,32] However, recent DF calculations[34] carried out for the RPM fluid in a slit-like pore using common compressibility route approach[10,51] with the assumption of a constant value of the dielectric constant throughout the entire system also led to an oscillatory behavior of the capacitance as a function of the pore width. The DF calculations suggest thus that such a behavior is primarily due to the interference of double layers at two pore walls.[34] Similar conclusion concerning the capacitance was also obtained by Henderson,[44] who used the MSA solution for the bulk RPM and an extended version of the linearized Poisson-Boltzmann approach. According to Henderson, the results of Refs. 34 and 44 do not imply that the polarization does not occur, it just is not necessary to produce oscillations in the capacitance.[44] Also, the dependence of capacitance versus pore width (for very narrow pores) was found to exhibit oscillating shape with two maxima by using computer simulations of model room temperature ionic liquid between flat walls, both of which were taken as three graphene layers.[42]

We should stress, however, that the theoretical results reported in Refs. 34 and 44 differ in several aspects. In particular, it is difficult to reconcile their predictions with respect to the behavior of capacitance for very narrow pores, to the positions of local density peaks and troughs, as well as to the number of oscillations and their magnitude. One can suspect that DF results of the double layer capacitance are very sensitive not only to the model details but also to the accuracy of a theoretical approach, as it happens, for example, with

the predictions concerning the existence of the vapor-liquid phase transition for the RPM under confinement and surface tension, or with the predictions of the dependence of electric double layer (EDL) capacitance on temperature.[18,19]

Quite recently Wang et al.[23,24] developed a new density functional approach to study RPM fluids in contact with charged surfaces. Although their method also belongs to the class of compressibility route approaches, but it uses special weighting procedure to evaluate the change of the direct correlation function of the system relative to that of a reference state. This weighting procedure can be particularly important in the case of strongly confined systems. A comparison with computer simulations showed that at temperatures higher than the bulk gas-liquid critical temperature, the theory is essentially more accurate in predicting the structure of the RPM fluid near a highly charged surface than previous compressibility route approaches. In particular, the approach is able to capture several fine structural features like layering of ion density and the charge inversion phenomena.

In this work our principal objective is to study adsorption of the RPM in slit-like pores of different width and to determine the dependence of the double layer capacitance on the pore width by using the developments of Wang et al.[23,24] Contrary to previous works,[34,44,52] we investigate the *differential* double layer capacitance that is a directly measurable quantity,[53,54] rather than the (integral) capacitance. We also pay attention to the questions that have been omitted in the previous studies, namely how the relationship of the differential double layer capacitance on the pore width is dependent on the value of the electrostatic potential at the wall and on the bulk fluid density. We believe, and it was already demonstrated in the case of ions in contact with a single wall,[23] that the DF approach used in the present work is one of the most accurate methods in describing the EDL at temperatures well above the critical temperature of the RPM under confinement.

II. THE MODEL AND THEORY

We consider adsorption of the restricted primitive model for electrolyte solutions in slit-like pores. The fluid consists of cations and anions of the valence Z_1 and Z_2, both species are modelled as charged hard spheres of equal diameter, σ. The solvent is not considered explicitly, it is a continuum of a given (relative) dielectric permittivity ϵ. The interactions between ions are given by

$$u_{\alpha\gamma}(r) = \begin{cases} \infty, & r < \sigma \\ \frac{e^2 Z_\alpha Z_\gamma}{4\pi\epsilon\epsilon_0} \frac{1}{r}, & r > \sigma \end{cases}, \qquad (1)$$

where $\alpha, \gamma = 1, 2$ and ϵ_0 is the vacuum permittivity. We assume that the dielectric permittivity ϵ is constant throughout the entire system.

The fluid is confined to a slit-like pore of the width H. The interaction of ions of species α along normal to the pore walls at $z = 0$ and at $z = H$ wall is described by the

potential

$$v^{(\alpha)}(z) = V_{hw}(z) + V_{el}^{(\alpha)}(z), \qquad (2)$$

where $V_{hw}(z)$, is the hard wall potential

$$V_{hw}(z) = \begin{cases} \infty, & \text{for } z < \sigma/2 \text{ or } z > H - \sigma/2 \\ 0, & \text{otherwise} \end{cases}, \qquad (3)$$

and $V_{el}^{(\alpha)}(z) = V_{el,1}^{(\alpha)}(z) + V_{el,1}^{(\alpha)}(H - z)$ with

$$\beta V_{el,1}^{(\alpha)}(z') = -2\pi l_B(\tilde{Q}/2)Z_\alpha z'. \qquad (4)$$

In the above $\beta = 1/kT$, $\tilde{Q} = Q/e$, Q is the surface charge density on *both* pore walls (we assume that the surface charge density of each wall is the same) and $l_B = e^2/(4\pi\epsilon\epsilon_0 kT)$ is the Bjerrum length. It is convenient to introduce the reduced "electrostatic" temperature as $T^* = \sigma/l_B$.

The confined fluid is in equilibrium with a bulk fluid. The bulk densities and chemical potentials are, respectively, $\rho_{b,\alpha}$ and μ_α, $\alpha = 1, 2$. The bulk densities of ionic species satisfy the electro-neutrality condition $Z_1\rho_{b,1} + Z_2\rho_{b,2} = 0$. The total bulk density is $\rho_b = \rho_{b,1} + \rho_{b,2}$.

The system is studied in the grand canonical ensemble. The equilibrium density profiles are obtained by minimizing the thermodynamic potential

$$\Omega = F + \sum_{\alpha=1,2} \int d\mathbf{r}\rho_\alpha(z)[v^{(\alpha)}(z) - \mu_\alpha] + \int d\mathbf{r}q(z)\Psi(z). \qquad (5)$$

In the above F is the free energy functional, $\rho_\alpha(z)$ is the local density of species α, and $q(z)$ is the charge density

$$q(z) = e \sum_{\alpha=1,2} Z_\alpha\rho_\alpha(z). \qquad (6)$$

The electrostatic potential, $\Psi(z)$, satisfies the Poisson equation

$$\nabla^2\Psi(z) = -\frac{1}{\epsilon\epsilon_0}q(z). \qquad (7)$$

The solution of the differential equation (7) is given in Refs. 2 and 55. It requires the choice of the boundary condition, i.e., of the value of the electrostatic potential at the wall, $V_0 = \Psi(z = 0) = \Psi(z = H)$. From the electro-neutrality condition of the system it follows that

$$Q + \int dz q(z) = 0. \qquad (8)$$

We recall that the surface charge density on a single pore wall is $Q/2$.

The principal task in DF theory is to derive an expression for the Helmholtz energy, F, as a functional of the local densities. We use here the theory from Refs. 23 and 24, and, therefore we present here the most essential points of the approach only. The free energy, F, is divided into an ideal, hard-sphere and residual electrostatic excess terms $F = F_{id} + F_{hs} + F_{el}$ (the direct Coulomb interactions have been already incorporated into the electrostatic potential). The ideal term is $F_{id} = \sum_{\alpha=1,2} \int d\mathbf{r}\rho_\alpha(\mathbf{r})[\ln \rho_\alpha(\mathbf{r}) - 1]$. The excluded volume (the hard-sphere) term, F_{hs}, is calculated according to

the Fundamental Measure Theory, cf. Ref. 56

$$F_{hs}/kT = \int d\mathbf{r} \left\{ -n_0 \ln(1-n_3) + \frac{n_1 n_2 - \mathbf{n}_{V1} \cdot \mathbf{n}_{V2}}{1-n_3} \right.$$

$$+ \frac{1}{36\pi} \left[n_3 \ln(1-n_3) + \frac{n_3^2}{(1-n_3)^2} \right]$$

$$\left. \times \frac{n_2^3 - 3n_2 \mathbf{n}_{V2} \cdot \mathbf{n}_{V2}}{n_3^3} \right\}, \qquad (9)$$

where n_i, $i = 0, 1, 2, 3$ and $\mathbf{n}_{Vj}$, $j = 1, 2$ are, respectively, scalar and vector total weighted densities. The total weighted densities are the sums of the weighted densities of individual species. The equations defining the weighted densities are given in Ref. 56. Following Wang *et al.*,[23,24] the residual electrostatic contribution F_{el},

$$F_{el}/kT = -\frac{1}{2} \sum_{\alpha,\gamma=1,2} \int d\mathbf{r}d\mathbf{r}' \Delta \bar{c}_{\alpha\gamma}(\mathbf{r}, \mathbf{r}')$$

$$\times [\rho_\alpha(\mathbf{r}) - \rho_{b,\alpha}][\rho_\gamma(\mathbf{r}') - \rho_{b,\gamma}], \qquad (10)$$

is determined using analytical expression for the direct correlation functions, $c_{\alpha\gamma}(\mathbf{r}, \mathbf{r}')$, that result from the Mean Spherical Approximation and the so-called "weighted correlation approach," WCA-k^2, see Refs. 23 and 24. We have

$$\Delta \bar{c}_{\alpha\gamma}(r) = \begin{cases} 0, & r > \sigma \\ u_{\alpha\gamma}(r)\left[1 - 2B_1\left(\frac{r}{\sigma}\right) + B_2\left(\frac{r}{\sigma}\right)^2\right], & r \leq \sigma \end{cases}, \qquad (11)$$

where

$$B_i(z) = \frac{\int dz' B^i(z')\kappa^2(z')\Theta(|z-z'|-\sigma)}{\int dz'\kappa^2(z')\Theta(|z-z'|-\sigma)}, \qquad (12)$$

and

$$B(z) = \frac{1 + \kappa(z)\sigma - \sqrt{1 + 2\kappa(z)\sigma}}{\kappa(z)\sigma}. \qquad (13)$$

In the above $\Theta(z)$ is the step-function and $\kappa(z)$ is the "local" Debye screening parameter,

$$\kappa^2(z) = \frac{\beta e^2}{\epsilon\epsilon_0} \sum_{\alpha=1,2} \rho_\alpha(z)Z_\alpha^2. \qquad (14)$$

At equilibrium the density profiles minimize thermodynamic potential, Ω, i.e.,

$$\frac{\delta\Omega}{\delta\rho_\gamma(\mathbf{r})} = 0, \quad \gamma = 1, 2. \qquad (15)$$

This condition leads to the equation for the density profiles,

$$\rho_\gamma(\mathbf{r}) = \exp[-\beta\mu_\gamma - \beta\lambda^{(\gamma)}(z)], \qquad (16)$$

where

$$\lambda^{(\gamma)}(z) = \frac{\delta[F_{hs} + F_{el}]}{\delta\rho_\gamma(z)} + v^{(\gamma)}(z) + eZ_\gamma\Psi(z). \qquad (17)$$

The theory reported above was tested against computer simulation results and a very good agreement was found.[23] Therefore, we are convinced that the DF results presented below should correctly capture all the discussed phenomena and that the theory is also more accurate than previous ones.

III. RESULTS AND DISCUSSION

The ion diameter, σ, is used as the unit of length, thus the dimensionless pore width and the distance are $H^* = H/\sigma$ and $z^* = z/\sigma$, respectively. The reduced densities are $\rho_{b,\alpha}^* = \rho_{b,\alpha}\sigma^3$. We recall that the reduced temperature is $T^* = \sigma/l_B$. Moreover, the reduced electrostatic potential and the reduced charge density at the wall are $V^* = eV_0/kT$ and $Q^* = Q\sigma^2/e$, respectively. Similar units have been used in several previous works, see, e.g., Ref. 51. Conversion coefficients from the reduced dimensionless units to volts and between other units one can find in Refs. 36, 37, and 51. All our calculations were carried out for an 1:1 electrolyte ($|Z^{(\alpha)}| = 1$) and majority of them (unless otherwise stated) at the temperature $T^* = 0.15$. This temperature is nearly twice of the critical RPM temperature, resulting from the energy-route MSA equation of state.[57]

A. Distribution of ions in pores, adsorption and selectivity

We begin our presentation with the examples of the density profiles of both ionic species in the pore of the width $H^* = 6$, the bulk fluid is at $\rho_b^* = 0.3$. Note that due to symmetry, only one-half of the profiles is plotted in Fig. 1. The consecutive curves in Figs. 1(a)–1(d) have been obtained for increasing values of V^*, keeping the bulk density of ions constant.

At low values of V^*, the counter-ions are mainly adsorbed at the pore walls (Fig. 1(a)), but at higher voltages the development of the second layer of counter-ions is observed at $z \approx 2.4$ (Figs. 1(b) and 1(c)). The co-ions are expelled from the contact layer with increasing V^* and
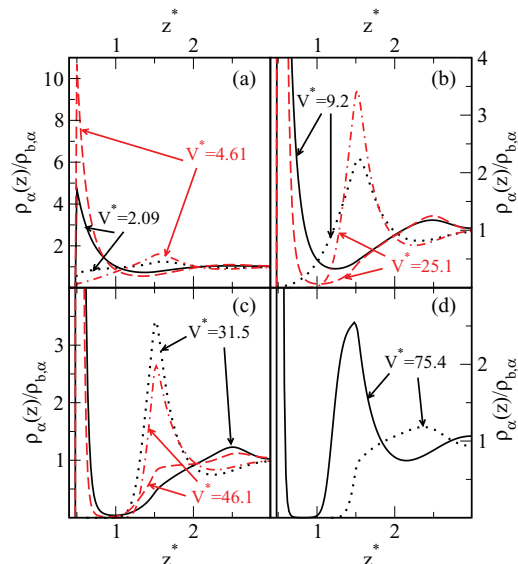

FIG. 1. Density profiles of ions in the pore $H^* = 6$ at different values of V^*. Solid and dashed lines are for counter-ions, dotted and dashed-dotted lines are for co-ions.

predominantly occupy the layer at $z^* \approx 1.5$ covering the contact layer of counter-ions beneath. This structure results from the effect of electric field yielding separation of ions, as well as from the attraction between counter-ions adsorbed on the pore walls and co-ions.

Up to $V^* \approx 30$ the height of the maximum of the profile describing co-ions increases with increasing voltage, but then it starts to decrease (Fig. 1(c)). This serves as a manifestation that the layer of co-ions reaches saturation at a certain value of V^*. The amount of co-ions in the layer at saturation depends on fluid density, temperature, pore width, and V^*. At high values of V^* the co-ion–wall repulsion prevails over the ion–ion attraction such that the height of the co-ion maximum decreases. Instantaneously, the counter-ions start to accumulate in the layer at $z^* \approx 1.5$. This change of structure does not mean that counter-ions substitute co-ions at this distance from the pore wall, rather the co-ions are expelled from the pore as the result of enhanced separation of two ionic species with increasing voltage. At even higher value of V^*, cf. Fig. 1(d), two dense counter-ion layers are formed on the pore walls whereas the co-ions tend to attain positions farther from the walls, over this counter-ion structure. The distribution of ions in Fig. 1(d) qualitatively resembles the so-called crowding structure of ionic liquid double layer observed by Bazant et al.[43] from Landau-Ginzburg-type continuum theory and simulations.

Attained structure of counter-ions and co-ions in the pore can be quantitatively characterized by adsorption isotherms, or, equivalently by the average densities of ions and selectivity isotherms. From the obtained density profiles we calculated the average densities of ion species in the pore,

$$A_\alpha = \frac{1}{(H-\sigma)} \int_{\sigma/2}^{H-\sigma/2} dz \rho_\alpha(z) \qquad (18)$$

and the selectivity coefficients,

$$S_\alpha = \frac{A_\alpha}{A}, \qquad (19)$$

where A is the total average ionic density, $A = A_1 + A_2$.

Figure 2(a) shows how the selectivity of adsorption depends on V^* for three pores of different width $H^* = 1.2$, 1.6, and 2.2. Each case is described by two branches, the lower branch is for co-ions, while the upper branch is for counterions. In the case of very narrow pores the change of the selectivity of adsorption with the applied voltage is very fast. Indeed, the pore of $H^* = 1.2$ contains almost counter-ions only already at $V^* \approx 6$. For $H^* = 1.6$ the voltage needed to attain the counter-ion selectivity of the order of 0.99 is higher, $V^* \approx 7.5$, whereas in the pore of the width $H^* = 2.2$, the voltage must be as high as 27.5 in order to attain the same selectivity. In wider pores, the separation of ions in terms of selectivity is incomplete unless one considers rather high values of V^*.

Figure 2(b) illustrates how the total average fluid density in the pores, A, changes with voltage at different bulk fluid density. For a narrow pore, $H^* = 1.2$, A grows fast in rather narrow window of V^*. Next, the total average density growth slows down with increasing V^* and a complete saturation is expected to occur at even higher voltage, at $V^* > 50$. Similar
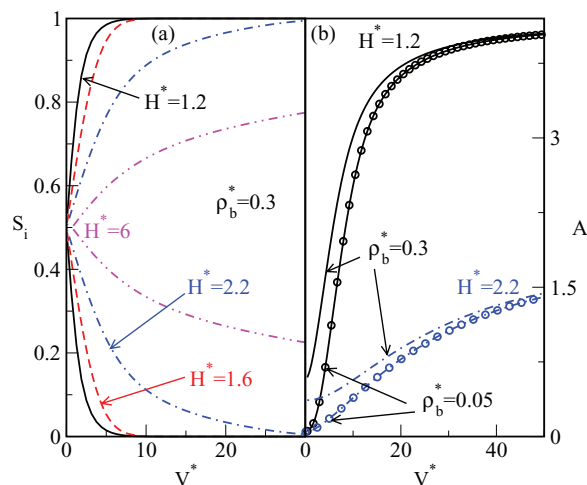

FIG. 2. (a) The dependence of the selectivity of adsorption of ionic species on applied voltage in the pores of different $H^* = 1.2$. Upper and lower sets of curves are for counter- and co-ions, respectively. (b) The dependence of total average density in the pore A on V^* for two pore widths and for two bulk fluid densities.

behavior is seen for $\rho_b^* = 0.05$ and 0.3. Moreover, the values for A close to saturation, are almost independent of the fluid density in the bulk, indicating that the pore attains its maximum capacity. The pore at this conditions is filled by counterions only (see Fig. 2(a)) that neutralize the pore walls charge in accordance with Eq. (8). For a wider pore, $H^* = 2.2$, trends for saturation are less pronounced, comparing to the previous case, within the range of V^* studied. Undoubtedly, the saturation will be reached at higher V^*. Also, the difference between the values of A for two different bulk fluid densities becomes smaller upon increasing V^*, indicating that the limit of maximum pore capacity is determined mostly by the pore width rather than by chosen bulk fluid density value. We will discuss other aspects of saturation of adsorption in narrow pores, namely in terms of surface charge density, slightly below.

B. Charge and capacitance dependence on electrostatic potential

Knowledge of the density profiles permits to proceed and to explore relation between the surface charge density and applied electrostatic potential. In particular, the capacitance (integral capacitance) is defined as the stored charge between two surfaces divided by the voltage,

$$C = Q/V_0. \qquad (20)$$

Another relation between the rate of change of the stored (or surface) charge divided by the rate of change of the voltage, or the electric surface potential,

$$C_d = \left(\frac{\partial Q}{\partial V_0}\right)_{\mu,T,H}, \qquad (21)$$

determines the "differential capacitance." It is the measurable property directly accessible from experiments.[53,54] Of course, if the stored charge is directly proportional to the voltage, i.e., the dependence between Q and V_0 is linear, then $C = C_d$. The
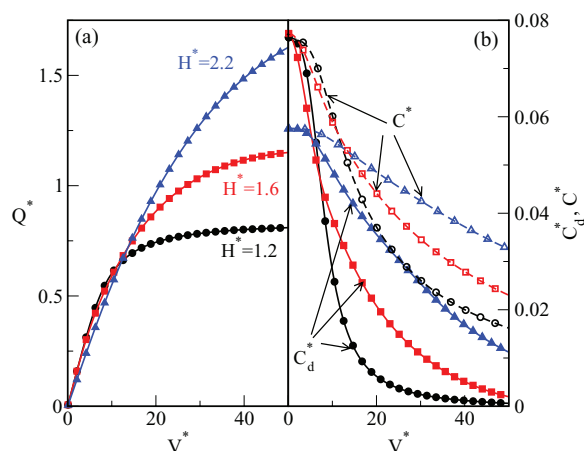
FIG. 3. The dependence of Q^* on the applied voltage (a) and the dependence of the differential capacitance (solid lines) and of integral capacitance (dashed lines) on V^* (b). The calculations are for different pore widths given in (a). The bulk density is $\rho_b^* = 0.3$.

reduced capacitance and the reduced differential capacitance, C^* and C_d^*, respectively, are defined as $C^* = (Q^*/V^*)$ and $C_d^* = \partial Q^*/\partial V^*$.

For the systems under study the dependence between Q^* and V^* is linear only for very small values of V^*. This point is illustrated in Fig. 3. Namely, in Fig. 3(a) the dependence of Q^* on the electrostatic potential for the pores of different width, $H^* = 1.2, 1.6$, and 2.2 is given. On the other hand, the differential and integral capacitances are shown in panel (b) of Fig. 3. Both capacitances coincide in the vicinity of $V^* = 0$, confirming linear dependence of surface charge density on V^* only in a very narrow interval.

For the narrowest pore of three cases considered ($H^* = 1.2$), the surface charge almost saturates attaining a plateau at high voltage, higher than $V^* \approx 30$. This is the region where the average density in the pore saturates as well, cf. Fig. 2(b). For a slightly wider pore there is no well pronounced plateau, but for $V^* > 40$ the growth of the surface charge with V^* is slow. However, for $H^* = 2.2$ a significant increase of the charge occurs for all investigated values of V^*.

The observed behavior can be explained as follows. For very narrow pores, the local density of counter-ions attains its maximum value at a certain value of V^* and further increase of counter-ion adsorption becomes impossible due to excluded volume effects. The existence of saturation of adsorption is expected for any pore width H^*. Consequently, for each pore width Q^* vs. V^* curve should possess a plateau, but at quite high values of V^*.

The dependence of the charge on voltage determines the behavior of capacitance and differential capacitance. Part (b) of Figure 3 shows the plots of differential double layer capacitances, C_d^*, on V^* for the systems from the panel (a) of this figure (Fig. 3(a)). We have also displayed here the integral capacitances, C^*, for the sake of comparison. We see that except for very low values of V^*, the differences between C_d^* and C^* are big. This is particularly manifested for the narrowest pore, $H^* = 1.2$, where for $V^* > 35$ the differential capacitance, C_d^*, is close to zero, while the values of C^* are even higher that the values of the differential capacitance for the pore of H^*

$= 2.2$. Similarly as in the case of Q^* vs. V^* dependence in Fig. 3(a), the differential capacitances curves cross, but now the crossings occur at lower values of V^*. On the other hand, the crossings of the capacitances C^* on V^* occur nearly at the same values of V^* as the crossings of Q^* vs. V^* curves.

The conclusion emerging from Fig. 3 is the following. While discussing the electric properties of double layers in porous systems under high voltage conditions and comparing theoretical predictions with experimental results, one should not assume that the behavior of C follows the behavior of C_d, because the differences between these quantities are significant. In what follows, we discuss the differential capacitance only, as it is the quantity directly accessible from experiments.

We would like to summarize this subsection with brief comments concerning the dependence of surface charge density on the electrostatic potential obtained by other authors for other model ionic fluids in narrow pores. Specifically, Kondrat et al.[37] obtained well defined plateau on the dependence of Q^* on V^* in their simulations of the RPM in slit-like metallic nanopores (cf. Fig. 1 of Ref. 37). The model interactions of that work include contributions coming from electrostatic images of single and pair type. The observed growth of surface charge on V^* was monotonous and almost linear before well defined threshold voltage. At higher values of V^*, the surface charge remained constant, i.e., it did not change with increasing applied voltage. On the other hand, Wu et al.[41] in the simulations of ionic liquid in slit-shaped subnanometer pores with polarizable walls, obtained weak trends for saturation of surface charge density with electrode potential (cf. Fig. 1(b) of that work), much less pronounced comparing to Ref. 37.

In contrast to these observations, the dependence of charge density on voltage in narrow pores presented by Jiang et al. (from their version of DF theory) for the model without electrostatic images' interactions does not exhibit trends for saturation, see Fig. 2 of Ref. 34. In view of the results given in Fig. 3(a), we can make conclusion that the accuracy of the DF theoretical constructions is crucial for the correct description of surface charge–electrostatic potential relation. It is worth mentioning that in spite of apparent difference in shape, the sequence of our Q^* vs. V^* curves for different pore width is similar to the results of Kondrat et al.[37] Evidently, the model in question and that of Ref. 37 are different. However, it seems that the way in which the adsorption of ions grows under the influence of increasing potential and the maximum capacity of a given pore determine overall shape of these dependencies.

C. Dependence of differential capacitance on pore width

As a preliminary to the discussion of the dependence of capacitance on pore width, we would like to describe briefly the available very recent results of other authors obtained by using theoretical methods for the models without electrostatic images. It was demonstrated that simple compressibility route DF approach[10,51] leads to the integral capacitance C of the RPM fluid as an oscillating function of H.[34] The observed behavior was attributed to the interference of the overlapping

electric double layers formed at opposing walls. According to given explanation, the maxima in capacitance appear when superposition of electric double layers from two walls is the most constructive, i.e., peaks coincide with peaks. This type of explanation of the behavior of C^* on H^* has also been used and shown to be successful in the interpretation of the simulation results for the model with explicit atomic structure of pore walls.[42] One drawback of the data presented in Ref. [34] is that the existence of the first peak for narrow pores is just a supposition, it is impossible to attribute certain values of capacitance for pores close to unity.

The oscillatory behavior of the capacitance C^* was also observed from a "modified" (the modification takes into account non-zero diameter of ions) linearized Poisson-Boltzmann approach.[44] For narrow pores the capacitance falls down to zero. Comparing the results of Refs. [34] and [44] one can realize striking differences, namely the C^* vs. H^* curves are shifted in phase and the period of oscillation is different. In the approach of Ref. [44] the values of capacitance do not depend on the applied electrostatic potential because of assumed linearization, whereas the curves in Figs. 3 and 4 of Ref. [34] correspond to a high value of electrostatic potential, V = 1.5 Volts. This can be one of the reasons of the discrepancy discussed above. Nevertheless, it seems that the difference between two above sets of results can be attributed to different accuracy of each theory. The Poisson-Boltzmann approach, modified by Henderson[44] is, of course, less accurate in describing the structure of EDL than DF approaches, but also the DF approach of Refs. [10], [34], and [51] is less accurate (in comparison with simulation results for the models that do not involve electrostatic images) than the theory of Wang et al.,[23,24] applied in the present study.

In Figure 4 we show the dependencies of the *differential* capacitance, C_d^*, on the pore width H^* for different values of the reduced electrostatic potential at the pore walls, V^*. The bulk density is constant and rather high, $\rho_b^* = 0.4$, in this series of calculations. We observe that the way of C_d^* changes with H^* depends on the value of electrostatic potential V^*. The most pronounced oscillations occur when the value of the electrostatic potential is low, $V^* = 0.5$, and close to the poten-

FIG. 5. The dependence of differential capacitance on pore width at a fixed electrostatic potential. The nomenclature of lines and symbols is given in panel (a).

tial of zero charge, $V_{PZC}^* = 0$ for the RPM model in question. Two well pronounced maxima are observed on the curve for pores in the interval between 1 and 5. Actually, we observed the third, weakly pronounced maximum for the pore slightly wider than $H^* = 5$.

The maxima are separated by a distance approximately equal to two diameters of ions. Similar value for characteristic distance is seen between two troughs. The value of the first maximum of capacitance located at $z^* = 1.28$, approximately is 1.6 times the value at the first trough. In contrast to this regular pattern, at a higher value of V^* ($V^* = 5$) we observe one maximum for very narrow, quasi-two-dimensional pore ($H^* \approx 1.08$). The second and third maximum are seen at $H^* \approx 1.6$ and 3.3, respectively. Still, the capacitance tends to a minimum for $H^* \rightarrow 1$. For higher values of V^* the repeated oscillations disappear. The capacitance C_d^* tends to zero for very narrow pores. Solely one maximum preserves for pores with $H^* > 2$, its height with respect to the asymptotic value for large values of H^* decreases, when the applied electrostatic potential increases. Its worth to remind that our results refer to the differential capacitance C_d^* (Eq. (21)), not to the "integral" capacitance C^*, Eq. (20), as in previous works.[34,44] We return to the discussion of the behavior of C_d^* for very narrow pores slightly below.

The next question is how the differential capacitance depends on the bulk fluid density. This issue is considered in Fig. 5, where we have compared the C_d^* vs. H^* curves evaluated at different values of V^* and at different bulk densities ρ_b^*. In each panel the results at a fixed value of V^* and for three values of bulk densities ρ_b^* are displayed. In Fig. 5(a) ($V^* = 0.5$) regular pattern is seen for three bulk fluids densities in question. However, the absolute values of capacitance decrease and the magnitude of oscillations becomes smaller for smaller bulk fluid density. For example, at $\rho_b^* = 0.2$ the second maximum of C_d^* at $H^* \approx 3.3$ is weakly pronounced.

In Fig. 5(b) ($V^* = 5$) the curves corresponding to two higher densities, 0.4 and 0.3, exhibit similar pattern with the
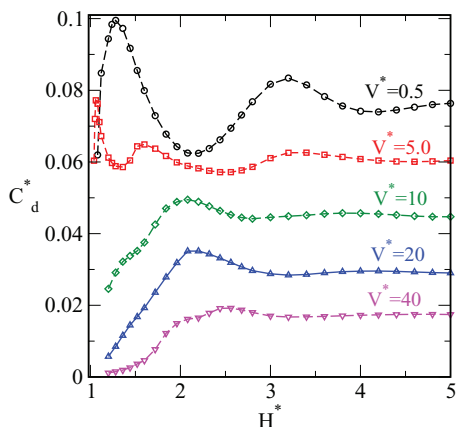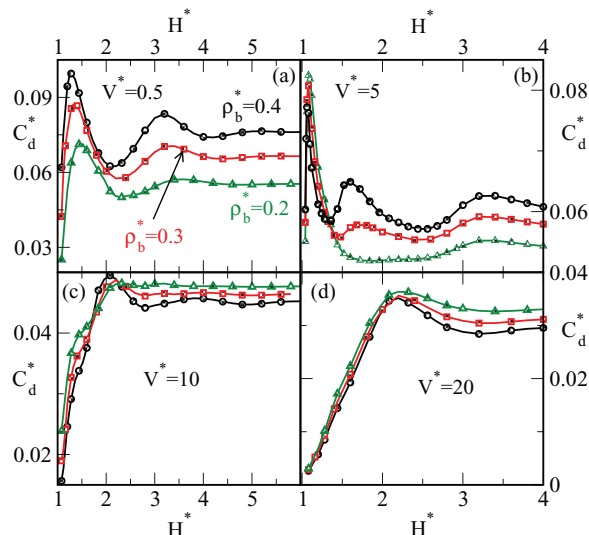

FIG. 4. The dependence of the differential capacitance on the pore width at different values of the electrostatic potential. The bulk ionic fluid total density is fixed at $\rho_b^* = 0.4$.
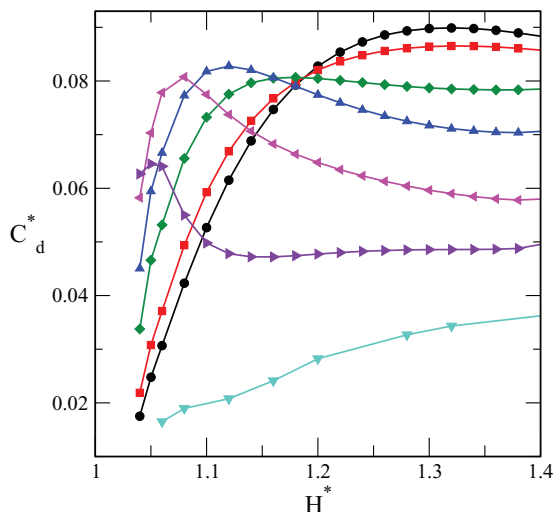
FIG. 6. The dependence of differential capacitance on pore width at a fixed electrostatic potential at $\rho_b^* = 0.3$ for very narrow pores. The consecutive curves are for $V^* = 0.5$ (circles), 1 (squares), 2 (diamonds), 3 (up triangles), 5 (left triangles), 7 (right triangles), and 10 (down triangles), from top to bottom at $H^* = 1.4$, respectively.

maximum of capacitance for quasi-two-dimensional pores. The value of capacitance at this maximum is higher at lower fluid density. In contrast, for wider pores the capacitance is lower for lower fluid density, in close similarity to the results given in panel (a) of this figure. Well pronounced oscillations appear again at this voltage. However, the maximum around $H^* = 1.5$ that is seen at high density, $\rho_b^* = 0.4$, decreases in magnitude for less dense fluid, $\rho_b^* = 0.3$, and disappears at even lower density, $\rho_b^* = 0.2$. For large values of V^* the differential capacitance tends to a minimum for very narrow pores, oscillations diminish and higher capacitance is obtained for lower bulk fluid densities, see Figs. 5(c) and 5(d). This is in contrast to what was observed at low voltage, cf. Fig. 5(a).

The shape of C_d^* vs. H^* curves for $V^* = 5$ is slightly puzzling. In order to clarify the issue in more detail, we performed additional calculations for very narrow pores (in the interval below $H^* = 1.4$ at $\rho_b^* = 0.3$) and made a fine scan for the values of applied surface potential. The results of calculations are given in Fig. 6. It appears that the first maximum of the curves C_d^* versus H^* exists for V^* starting from 0.5 up to 7. Its value substantially decreases with increasing V^*, while its position tends to H^* close to unity, i.e., for almost two-dimensional pores. The maximum disappears in the region of V^* between 7 and 10. In summary, our data show that for entire range of values of V^* studied, the differential capacitance tends to a minimum in very narrow pores. Of course, both C^* and C_d^* should vanish for $H^* = 1$ (strictly speaking for H^* lower than 1), because ions cannot enter such narrow pores and thus the charge on the walls is zero. It does not mean, however, that $\lim_{H^* \to 1^+} C_d^*(H^*)$ must vanish.

Now, we would like to make summarizing insight in order to get hints for the explanation of observed trends of the behavior of C_d^*. For the model under study, the differential capacitance depends on four parameters: the bulk fluid density (or equivalently the chemical potentials of ions), temperature,

the surface charge density on the wall and on the pore width. For wide pores the double layers at the opposite pore walls are independent and the interference of the overlapping electric double layers is vanishing. Thus, the capacitance is constant as a function of H^*, for all wide pores with non-overlapping electric double layers at fixed values of ρ_b^*, T^* and V^*. From the point of view of microscopic structure in this regime, one must consider a pore in which the distribution of ions is characterized by the bulk density in its central part and work at V^* such that the EDL at each pore wall is narrower comparing to half width of the pore. At such conditions, the double layer will be composed of counter-ions and co-ions. When the pore width decreases, the interference of the double layers occurs and starts to play significant role. Extension of the EDL can be regulated by fluid density, temperature, and electrostatic potential of the wall.

As we have already shown (cf. the discussion of Figs. 2(a), 2(b), and 3(a)) in the case of narrow pores, the pore space contains counter-ions as well as co-ions at low voltage. With increasing voltage the amount of adsorbed co-ions decreases, and in the limit of very high voltages the entire pore is filled with counter-ions only, until maximum capacity of the pore is attained. Simultaneously, the charge Q^* grows and in the limiting case its saturation is reached. This behavior of capacitance mirrors those trends and C_d^* tends to zero at very high voltage. For narrower pores the adsorbed film attains its maximum density at lower values of V^* comparing to slightly wider pores.

At a low voltage a narrow pore is not completely filled and the structure of the fluid results from the interference of the double layers at two pore walls. If $V^* = 0$, the local densities of co- and counter-ions are identical, $Q^* = 0$ and the structure is determined by excluded volume effects. At nonzero electrostatic potential V^* the ionic species are separated and the profiles of co- and counter-ions are different. The structure of EDL in the pore results from an interplay between volume exclusion and screened electrostatic interactions and leads to the profiles discussed, for example, in the case of Fig. 1. The density profiles minimize the thermodynamic potential Ω and satisfy the electroneutrality condition. We believe that the mechanism of the formation of the maxima and troughs of C_d^* on H^* dependencies is in the constructive or destructive interference of the EDL from two walls.[34,42] Unfortunately, similarly to previous publications,[34,44] the lack of computer simulation data for the model in question does not permit us to prove it unequivocally.

D. Temperature dependence of differential capacitance

Finally, we would like to study the temperature dependence of the double layer capacitance for the model in question. Computer simulations of a RPM fluid near a charged hard wall carried out by Boda and co-workers[48–50] for a wide temperature interval and from low to intermediate densities showed that the temperature dependence of the capacitance is characterized by a peculiar shape. Namely, the capacitance has a negative slope at high temperatures and a positive slope at low temperatures, i.e., the capacitance versus temperature
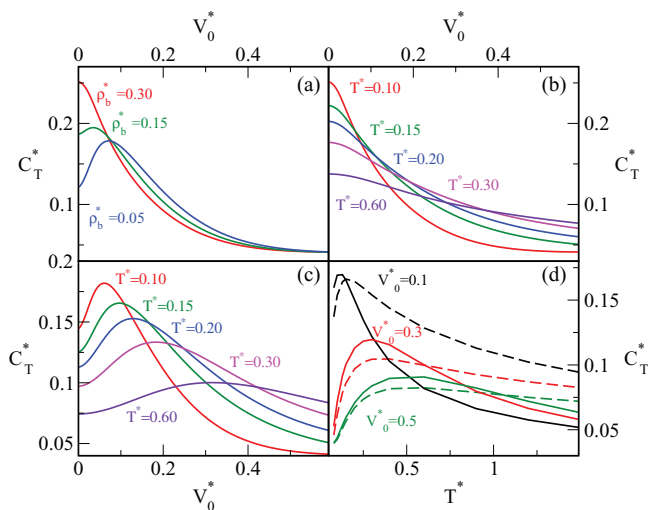
FIG. 7. (a) The dependence of C_T^* on V_0^* at three different bulk fluid densities and at $T^* = 0.1$. (b) and (c) The dependence of C_T^* on V_0^* at different temperatures given in the figure. (b) $\rho_b^* = 0.30$ and (c) $\rho_b^* = 0.079$. (d) Temperature dependence of C_T^* for $V_0^* = 0.1$ (black lines), $V_0^* = 0.3$ (red lines), and $V_0^* = 0.5$ (green lines). The results are for $\rho_b^* = 0.30$ (solid lines) and for $\rho_b^* = 0.079$ (dashed lines). All the calculations were performed for $H^* = 12$.

curve exhibits a maximum at a certain temperature. On the other hand, an increase of capacitance values with temperature, for ionic liquids in certain temperature interval, has been documented experimentally.[58] Common density functional compressibility route approaches,[10–15,51] have failed to reproduce simulation data. However, the use of the energy route DF theory[16–19] was quite successful in explaining the temperature dependence of the capacitance of the electrical double layer. The principal issue in this respect is to have theoretical tools that describe ionic distribution in the vicinity of the charged surface adequately or in other words capture correlations between ions in the presence of the external electric field accurately.

Thus it is important to explore whether the theory employed in this work[23,24] is capable in reproducing the existence of a maximum on the double layer capacity vs. temperature curve. In order to make a comparison of the present results with those obtained previously[18,19,48–50] we introduce the reduced capacitance C_T^*, defined as $C_T^* = (1/2T^*)C_d^*$ and plot it against V_0^*, $V_0^* = V^*(T^*/4\pi)$. The reason for that is the following. The definition of the reduced dimensionless potential, V^*, already contains the temperature and to obtain a plot of the temperature dependence of the capacitance in the scale used in Refs. 18 and 19, we have to account for that.

In Figure 7, we show how C_T^* changes with the voltage at a fixed temperature but for different bulk fluid density (part (a)), as well at a fixed bulk fluid density, but at different temperatures (parts (b) and (c)). In order to compare the results with previous ones[18,19,48–50] at a qualitative level, our calculations have been carried out for a rather wide pore, $H^* = 12$. Nevertheless, one should remember that Refs. 18 and 19 present integral (not differential) capacities and that those calculations were carried out at a constant surface charge.

Part (b) of Fig. 7 is for high bulk density, $\rho_b^* = 0.3$, while part (c) is for much lower bulk density, $\rho_b^* = 0.079$.

The latter value is the same as one of the densities studied in Refs. 18 and 19. Finally, Fig. 7(d) displays the temperature dependence of C_T^* at $\rho_b^* = 0.3$ and $\rho_b^* = 0.079$. It can be seen that unlike the "classical" compressibility route approaches,[10–15] the theory used in this study predicts the existence of a maximum of capacitance vs. temperature curve. At a fixed T^* the dependence of C_T^* on V_0^* is camel-shaped, providing that the bulk density is not too high (Fig. 7(a)). At high density this dependence is bell-shaped. These trends are in agreement with the results of Ref. 51 Similarly, for a constant bulk density (Figs. 7(b) and 7(c)) the dependence of C_T^* on V_0^* is camel-shaped at all temperatures studied, providing that the bulk density is not too high. The curves C_T^* vs. temperature possess maxima at low and higher bulk density. The maximum of the differential capacitance is more pronounced at lower voltages. Note that at higher temperatures ($T^* > 1$) the sequence of the curves evaluated for different values of V_0^* at low and higher bulk densities is reversed. For $\rho_b^* = 0.3$ the highest capacitance C_T^* is at $V_0^* = 0.5$, while for $\rho_b^* = 0.079$ – at $V_0^* = 0.1$. The data given in Fig. 7 are in qualitative agreement with the results of Refs. 18, 19, and 48–50.

IV. SUMMARY AND CONCLUDING REMARKS

In this study we investigated the microscopic structure, adsorption, and electric properties of the restricted primitive model for an ionic fluid confined to slit-like pores with charged walls. Similarly to previous works in the framework of density functional theory, it has been assumed that the dielectric susceptibility is constant throughout the system, or, in other words, the effects of electrostatic images are not included into the model for potential energy. Our principal findings concern the dependence of the surface charge density, Q^*, on applied electrostatic potential, V^*. The surface charge density follows from the density profiles of ions in such inhomogeneous systems. The profiles minimize the grand thermodynamic potential and satisfy the electroneutrality condition. It was found that the surface charge density saturates with increasing electrostatic potential for different pore width. This saturation is related to adsorption of ions in the pores. With increasing voltage the adsorption of ions in a pore reaches its maximum capacity, such that for high voltages the charge density becomes independent on V^*. The charge as a function of V^* yields the differential capacitance. All the results presented suggest that the observed changes of the differential capacitance result from a quite complex interplay between different factors (e.g., the pore width, bulk fluid density, voltage on the walls and temperature).

We have shown that the number of oscillations of the differential capacitance on pore width and their magnitude decrease at high values of the electrostatic potential. Moreover, for very narrow pores the differential capacitance tends to a minimum value, in close similarity to Ref. 44 In our opinion, the oscillatory dependence of the capacitance as a function of the pore width can be explained in terms of the interference of electric double layers formed at each pore walls. This mechanism has been documented in very detail in Refs. 34 and 42 to interpret theoretical[34] and computer simulation data.[42]

Reliability of the results obtained from a given theoretical approach crucially depends on its accuracy. Among all existing "compressibility route" density functional theories, the approach proposed by Wang *et al.*[23, 24] seems to be the most accurate at temperatures higher than the bulk critical temperature of an RPM fluid. This approach not only satisfactory reproduces the simulation results for local densities of a fluid in contact with a single wall[23, 24] but also leads to qualitatively correct description of the temperature dependence of the double layer capacitance.[48–50] Therefore, in our opinion, it should also lead to much more accurate predictions of the electric capacitance in narrow pores. On the other hand, there is room for improvement of modelling of this study to put it closer to the models involving dielectric discontinuity at the solid–fluid boundary, e.g., Refs. 36, 37 as well as the procedure. Some of these issues will be considered in a future work in our laboratory.

[1]R. Kjellander and S. Sarman, Mol. Phys. **70**, 215 (1990).
[2]M. Lozada-Cassou, in *Fundamentals of Inhomogeneous Fluids*, edited by D. Henderson (Marcel Dekker, New York, 1992), Chap. 8.
[3]M. Plischke and D. Henderson, J. Chem. Phys. **88**, 2712 (1988).
[4]J. F. Lutsko, Adv. Chem. Phys. **144**, 1 (2010).
[5]O. Pizio and S. Sokołowski, "Advances in the theoretical description of solid-electrolyte solution interfaces," in *Solid State Electrochemistry II*, edited by V. V. Kharton (Wiley-VCH, Weinheim, 2011), Chap. 3, pp. 73–124.
[6]B. M. Malo, L. Salazar, S. Sokołowski, and O. Pizio, J. Phys.: Condens. Matter **12**, 8785 (2000).
[7]C. N. Patra, J. Phys. Chem. B **114**, 10550 (2010).
[8]K. Bucior, A. Patrykiejew, O. Pizio, and S. Sokołowski, J. Colloid Interface Sci. **259**, 209 (2003).
[9]S. Jain, A. Dominik, and W. G. Chapman, J. Chem. Phys. **127**, 244904 (2007).
[10]Z. Tang, L. E. Scriven, and H. T. Davis, J. Chem. Phys. **97**, 9258 (1992).
[11]R. Kjellander and H. Greberg, J. Electroanal. Chem. **450**, 233 (1998).
[12]C. N. Patra and A. Yethiraj, J. Phys. Chem. B **103**, 6080 (1999).
[13]D. Boda, D. Henderson, R. Rowley, and S. Sokołowski, J. Chem. Phys. **111**, 9382 (1999).
[14]Y.-X. Yu, J.-Z. Wu, and G.-H. Gao, J. Chem. Phys. **120**, 7223 (2004).
[15]D. Gillespie, W. Nonner, and R. Eisenberg, Phys. Rev. E **68**, 031503 (2003).
[16]O. Pizio, A. Patrykiejew, and S. Sokołowski, J. Chem. Phys. **121**, 11957 (2004).
[17]O. Pizio and S. Sokołowski, J. Chem. Phys. **122**, 144707 (2005).
[18]J. Reszko-Zygmunt, S. Sokołowski, D. Henderson, and D. Boda, J. Chem. Phys. **122**, 084504 (2005).
[19]J. Reszko-Zygmunt, S. Sokołowski, and O. Pizio, J. Chem. Phys. **123**, 016101 (2005).
[20]A. Patrykiejew, S. Sokołowski, and O. Pizio, Condens. Matter Phys. **14**, 13603 (2011).
[21]E. Waisman and J. L. Lebowitz, J. Chem. Phys. **56**, 3086 (1972); **56**, 3093 (1972).
[22]L. Blum, Mol. Phys. **30**, 1529 (1975).
[23]Z. Wang, L. Liu, and I. Neretnieks, J. Phys.: Condens. Matter **23**, 175002 (2011).
[24]Z. Wang, L. Liu, and I. Neretnieks, J. Chem. Phys. **135**, 244107 (2011).
[25]J. R. Miller and P. Simon, Science **321**, 651 (2008).
[26]J. R. Miller, R. A. Outlaw, and B. C. Holloway, Science **329**, 1637 (2010).
[27]S. Mitani, M. Sathish, D. Rangappa, A. Unemoto, T. Tomai, and I. Honma, Electrochim. Acta **68**, 146 (2012).
[28]T. A. Centeno, O. Sereda, and F. Stoeckli, Phys. Chem. Chem. Phys. **13**, 12403 (2011).
[29]J. J. Yoo, K. Balakrishnan, J. Huang, V. Meunier, B. G. Sumpter, A. Srivastava, M. Conway, A. L. Mohana Reddy, J. Yu, R. Vajtai, and P. M. Ajayan, Nano Lett. **11**, 1423 (2011).
[30]L. Wei, M. Sevilla, A. B. Fuertes, R. Mokaya, and G. Yushin, Adv. Funct. Mater. **22**, 827 (2012).
[31]J. Chmiola, G. Yushin, Y. Gogotsi, C. Portet, P. Simon, and P. L. Taberna, Science **313**, 1760 (2006).
[32]C. Largeot, C. Portet, J. Chmiola, P.-L. Taberna, Yu. Gogotsi, and P. Simon, J. Am. Chem. Soc. **130**, 2730 (2008).
[33]C. Merlet, B. Rotenberg, P. A. Madden, P.-L. Taberna, P. Simon, Yu. Gogotsi, and M. Salanne, Nature Mater. **11**, 306 (2012).
[34]D. Jiang, Z. Jin, and J.-Z. Wu, Nano Lett. **11**, 5373 (2011).
[35]N. Georgi, A. Kornyshev, and M. Fedorov, J. Electroanal. Chem. **649**, 261 (2010).
[36]S. Kondrat and A. Kornyshev, J. Phys.: Condens. Matter **23**, 022201 (2011).
[37]S. Kondrat, N. Georgi, M. V. Fedorov, and A. A. Kornyshev, Phys. Chem. Chem. Phys. **13**, 11359 (2011).
[38]Y. Shim and H. Kim, ACS Nano **4**, 2345 (2010).
[39]B. Skinner, T. R. Chen, M. S. Loth, and B. I. Shklovskii, Phys. Rev. E **83**, 056102 (2011).
[40]J. W. Lee, R. H. Nilson, J. A. Templeton, S. K. Griffiths, A. Kung, and B. M. Wong, J. Chem. Theory Comput. **8**, 2012 (2012).
[41]P. Wu, J. Huang, V. Meunier, B. G. Sumpter, and R. Qiao, J. Phys. Chem. Lett. **3**, 1732 (2012).
[42]G. Feng and P. T. Cummings, J. Phys. Chem. Lett. **2**, 2859 (2011).
[43]M. Z. Bazant, B. D. Storey, and A. A. Kornyshev, Phys. Rev. Lett. **106**, 046102 (2011).
[44]D. Henderson, J. Colloid Interface Sci. **374**, 345 (2012).
[45]D. Jiang, Z. Jin, D. Henderson, and J.-Z. Wu, J. Phys. Chem. Lett. **3**, 1727 (2012).
[46]L. D. Landau and E. M. Lifshits, *The Classical Theory of Fields* (Addison-Wesley, Reading, MA, 1962).
[47]L. Blum, J. Phys. Chem. **81**, 136 (1977).
[48]D. Boda, D. Henderson, and K. Y. Chan, J. Chem. Phys. **110**, 5346 (1999).
[49]D. Boda, D. Henderson, K. Y. Chan, and D. T. Wasan, Chem. Phys. Lett. **308**, 473 (1999).
[50]M. Holovko, V. Kapko, D. Henderson, and D. Boda, Chem. Phys. Lett. **341**, 363 (2001).
[51]D. E. Jiang, D. Meng, and J.-Z. Wu, Chem. Phys. Lett. **504**, 153 (2011).
[52]D. Henderson, S. Lamperski, Z. Jin, and J.-Z. Wu, J. Phys. Chem. B **115**, 12911 (2011).
[53]A. P. Pchelnikov, A. D. Sitnikov, I. K. Marshakov, and V. V. Losev, Electrochim. Acta **26**, 591 (1981).
[54]C. M. Pettit, P. C. Goonetilleke, and D. Roy, J. Electroanal. Chem. **589**, 219 (2006).
[55]D. Henderson, P. Bryk, S. Sokołowski, and D. T. Wasan, Phys. Rev. E **61**, 3896 (2000).
[56]Y.-X. Yu and J.-Z Wu, J. Chem. Phys. **117**, 10156 (2002).
[57]J. Jiang, L. Blum, O. Bernard, and J. M. Prausnitz, Mol. Phys. **99**, 1121 (2001).
[58]V. Lockett, R. Sedev, J. Ralston, M. Horne, and T. Rodopoulos, J. Phys. Chem. C **112**, 7486 (2008).